

# SCIENTIFIC REPORTS



OPEN

## Analysis of Side-band Inequivalence

Sina Khorasani

Frequency shifts of red- and blue-scattered (Stokes/anti-Stokes) side-bands in quantum optomechanics are shown to be counter-intuitively unequal, resulting in an unexpected symmetry breaking. This difference is referred to as Side-band Inequivalence (SI), which normally leans towards red, and being a nonlinear effect it depends on optical power or intracavity photon number. Also there exists a maximum attainable SI at an optimal operation point. The mathematical method employed here is a combination of operator algebra equipped with harmonic balance, which allows a clear understanding of the associated nonlinear process. This reveals the existence of three distinct operation regimes in terms of pump power, two of which have immeasurably small SI. Compelling evidence from various experiments sharing similar interaction Hamiltonians, including quantum optomechanics, ion/Paul traps, electrooptic modulation, Brillouin scattering, and Raman scattering unambiguously confirm existence of a previously unnoticed SI.

The nonlinearity of optomechanical interaction<sup>1–10</sup> causes scattering of incident photons with the annihilator  $\hat{a}$  from the cavity unto either red- or blue-shifted photons through annihilation or generation of a cavity phonon with the annihilator  $\hat{b}$ , giving rise to the first-order mechanical side-bands. Taking the optical frequency  $\omega$  to be at a detuning  $\Delta = \omega_c - \omega$  from cavity resonance  $\omega_c$ , the  $\nu$ -th order sidebands are naturally expected to occur at the detunings  $\Delta_{\pm\nu} = \Delta \mp \nu\Omega$ , where  $\Omega$  represents the mechanical frequency. As a result, the first-order mechanical side-bands of scattered red  $\Delta_{+1}$  and blue  $\Delta_{-1}$  processes must average out back to the original pump detuning  $\Delta$ .

Defining the deviation of this average from  $\Delta$ , as  $\delta = \frac{1}{2}(\Delta_{+1} + \Delta_{-1}) - \Delta$ , then one may normally expect  $\delta = 0$ . A non-zero  $\delta$  would have otherwise implied the so-called Side-band Inequivalence (SI). This type of asymmetry appears to have a classical nonlinear nature, and is illustrated in Fig. 1.

There is, however, another well-known type of side-band asymmetry between the red and blue side-bands in the context of optomechanics, which has a quantum nature and may be used for instance to accurately determine the absolute temperature through a reference-free optomechanical measurement<sup>11,12</sup>. This is based on the ratio of Stokes to anti-Stokes Raman transition rates, which is equal to  $\exp(\hbar\Omega/k_B T)$  where  $k_B$  is the Boltzmann's constant and  $T$  is the absolute temperature<sup>13,14</sup>. Also illustrated in Fig. 1, clearly, SI is quite different from this type of side-band asymmetry.

While both time-reversal symmetry and energy conservation are fundamentally preserved in this scattering process, a nonlinear analysis of quantum optomechanics using the recently developed method of higher-order operators<sup>15–19</sup> necessitates a slight difference among detunings of blue and red-scattered photons, the amount of which was initially found to increase roughly proportional to the intracavity photon number  $\bar{n}$ . Here,  $\bar{n}$  is defined as the steady-state mean-value of the number operator  $\hat{n} = \hat{a}^\dagger \hat{a}$ .

Surprisingly enough, this disagreement satisfying  $\delta \neq 0$  does not violate the energy conservation law, actually allowed by the finite cavity linewidth as well as the single-photon/single-phonon nature of the process involved. Moreover, the time-reversal symmetry is also preserved.

Among the pool of available experimental data, only a handful of side-band resolved cavities reveal this disagreement<sup>15</sup>. Some initial trial experiments recently done at extremely high intracavity photon numbers  $\bar{n}$ , and/or extremely large single-photon optomechanical interaction rates  $g_0$ , though, failed to demonstrate its existence. This may raise the speculation that whether SI would have been merely a mathematical artifact, or something has been missing due to not doing the operator analysis to the highest-order.

A careful analysis of this phenomenon, however, confirms the latter, thus classifying the quantum optomechanical interaction into three distinct regimes with different behaviors:

- Fully Linear: This regime can be investigated using the lowest-order analysis and first-order operators, which is conventionally done by linearizing the Hamiltonian around equilibrium points. This will require the

Vienna Center for Quantum Science and Technology, Boltzmanngasse 5, 1090, Vienna, Austria. Correspondence and requests for materials should be addressed to S.K. (email: [sina.khorasani@ieee.org](mailto:sina.khorasani@ieee.org))

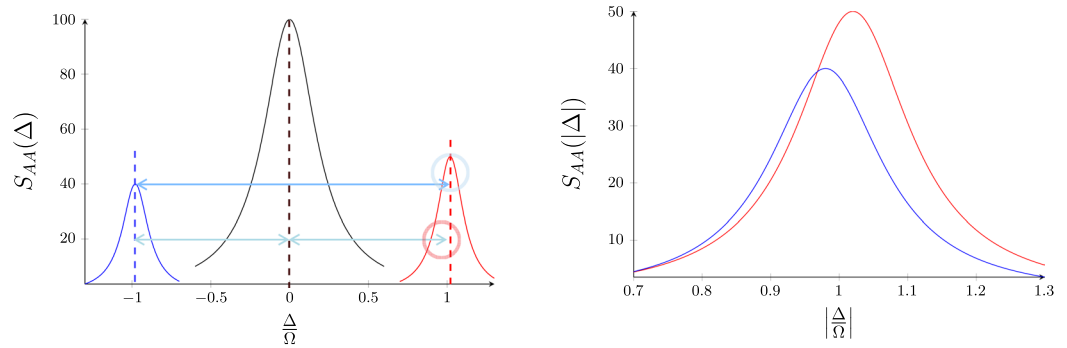


**Figure 1.** Illustration of two basic symmetry breakings in a hypothetical quantum optomechanical cavity at resonant pump, and in absence of cooling tone: (left) separated side-bands in a heterodyne setup; (right) zoom out of overlapping side-bands in a homodyne detection around mechanical frequency with  $|\Delta| = \Omega$ . The red detuning exceeds that of blue detuning, shown in pale red circle, corresponding to the side-band inequivalence (pale red circle), and also the height of red peak exceeds that of blue peak, corresponding to side-band asymmetry (pale blue circle). Here,  $S_{AA}(\Delta)$  represents the spectral noise density. Blue and red Lorentzian linewidths are  $0.1\Omega$ , while the central resonance has a linewidth of  $0.2\Omega$ . Side-band Inequivalence is chosen to be  $\delta = \delta/\Omega = 0.02$  towards red side-band.

four-dimensional basis of first-order ladder operators  $\{\hat{a}, \hat{a}^\dagger, \hat{b}, \hat{b}^\dagger\}$  and is indeed quite sufficient to understand many of the complex quantum optomechanical phenomena<sup>20</sup>.

- Weakly Nonlinear: This regime requires higher-order operator analysis of at least second-order. This can be done using the three-dimensional reduced basis<sup>15,20</sup> given as  $\{\hat{a}, \hat{a}\hat{b}, \hat{a}\hat{b}^\dagger\}$ .
- Strongly Nonlinear: Full understanding of this interaction regime requires the highest-order analysis using third-order operators. Referred as to the minimal basis<sup>15,20</sup>, the convenient reduced choice is the two-dimensional basis  $\{\hat{n}^2, \hat{n}\hat{b}\}$ .

In the latter regime, the behavior of governing equations is in such a way that a fully-linearized analysis of fluctuations mostly happens to work. This definitely sounds strange, unless we note that for the strongly non-linear regime, the optical pump level is so strong that the quantumness of intracavity photons disappear and we can do the replacements  $\hat{n}(t) \rightarrow \bar{n}(t)$  and  $\hat{a}(t) \rightarrow e^{i\Delta t}a(t)$ . Once the steady-state is reached, the minimal basis reduces to  $\bar{n}^2, \bar{n}\hat{b}$ . It is easy to see that  $\bar{n}$  stays almost constant so that mechanics is still quantized and expressed via  $\hat{b}$ . Based on the Langevin's equations for classical electromagnetic field  $a(t)$  and quantized mechanics  $\hat{b}(t)$  it is easy to see that the only surviving frequencies are  $\Delta \pm \Omega \pm 2\Omega \pm \dots$ . Hence, quantumness of optics is absolutely necessary for the SI to occur, and this disappears when the optical pump is so strong that the electromagnetic field can be treated classically.

Side-band Inequivalence is essentially forbidden in the fully linear regime, and it also quickly fades away in the strongly nonlinear regime. But it may only happen in the weakly nonlinear regime. This is now also confirmed both by the higher-order operator method and extensive calculations. It typically does not exceed one part in million to one part in ten thousand in solid state quantum optomechanics, and therefore, it is a very delicate phenomenon and elusive to observe. As it will be shown, other experiments such as Raman scattering may instead exhibit much stronger inequivalences.

This letter provides a direct route towards clear understanding of this complex nonlinear phenomenon. Using a combination of operator algebra and harmonic balance (used in analysis of laser diodes)<sup>21</sup>, we obtain a closed form expression for SI  $\delta$  as a function of intracavity photon number  $\bar{n}$ , which is expected to be valid through all three above operation regimes, and for any arbitrarily chosen set of optomechanical parameters. Not only the findings of this work reproduce the approximate linear expression found earlier through second-order operators<sup>15</sup> for the weakly nonlinear regime, but also we can show that there is an optimal point at which the SI attains a maximum. Moving away from the optimal point, both at the much smaller and much larger pump rates,  $\delta$  attains much smaller values, tending to zero in the limit of very large  $\bar{n}$ . An analytical treatment of nonlinear optomechanical equations based on breathing solutions is also presented, which again confirms the existence of inequivalence towards red and is presented in the Supplementary Information.

This will be greatly helpful to designate the investigation range of experimental parameters given any available optomechanical cavity. Furthermore, it marks a clear and definable border among the three above-mentioned operation regimes.

## Results

The analysis of SI proceeds with considering the behavior of optomechanical cavity under steady-state conditions. We will focus only on the first-order side-bands and discard all other contributions coming from or to the second- and higher-order side-bands. We consider a single-frequency pump with ideally zero linewidth at a given detuning  $\Delta$ , which normally gives rise to two stable blue- and red- side-bands. Hence, the time-dependence of the photon annihilator will look like

$$\hat{a}(t) = \hat{a}_0 e^{i\Delta t} + \hat{a}_b e^{i(\Delta - \Omega + \frac{1}{2}\delta)t} + \hat{a}_r e^{i(\Delta + \Omega + \frac{1}{2}\delta)t} + \dots, \tag{1}$$

where  $\hat{a}_0$ ,  $\hat{a}_b$ , and  $\hat{a}_r$  respectively correspond to the central excitation resonance at pump frequency, and blue- and red-detuned side-bands. In the weak coupling regime where  $g = g_0 \sqrt{\bar{n}} \ll \Omega$ , the  $n + 1$ -th order side-band is typically  $(g/\Omega)^n$  times weaker in amplitude than the 1st-order side-band. This means, for instance, that the second-order side-band is  $g/\Omega$  weaker than the first-order side-bands. In that sense, their respective contributions and significance diminish very rapidly with their growing order. So, there is good reason to agree that the truncation in (1) up to the first-order side-bands is a rather acceptable approximation. Inclusion of 2nd-order terms such as  $\hat{a}_{bb} e^{i(\Delta - 2\Omega + \delta)t}$  and  $\hat{a}_{rr} e^{i(\Delta + 2\Omega + \delta)t}$ , will result in minor modification of following expressions. It has to be noticed that the red and blue time dependences of  $n$ -th order processes must be  $e^{i(\Delta - n\Omega + \frac{n}{2}\delta)t}$  and  $e^{i(\Delta + n\Omega + \frac{n}{2}\delta)t}$ , showing that the associated SI with the  $n$ -th order side-bands should be  $n\delta$ .

We here furthermore have ignored the symmetrical movement of side-bands which should correspond to the optomechanical spring effect  $\delta\Omega$ <sup>1,3</sup>, but this correction is zero at  $\Delta = 0$  while  $\delta$  is independent of  $\Delta$  (in Supplementary Information we show that contribution of this term is insignificant). It is the asymmetric movements of side-bands which gives rise to SI. In order to do so, it would have been enough to take the ansatz  $\hat{a}(t) = \hat{a}_0 e^{i\Delta t} + \hat{a}_b e^{i(\Delta - \varpi + \frac{1}{2}\delta)t} + \hat{a}_r e^{i(\Delta + \varpi + \frac{1}{2}\delta)t} + \dots$  instead, with  $\varpi = \Omega + \delta\Omega$  being the shifted mechanical frequency due to the optomechanical spring effect.

The steady-state time-average of central excitation satisfies  $\hat{a}_0 = \sqrt{\bar{n}}$ , where  $\bar{n}$  can be determined by solution of a third-order algebraic equation once the optical power pump rate  $P_{\text{op}}$ , detuning  $\Delta$ , external coupling  $\eta$  and all other optomechanical parameters are known. The standard set of basic optomechanical parameters needed here are mechanical frequency  $\Omega$ , optical decay rate  $\kappa$ , and mechanical decay rate  $\Gamma$ . Therefore, the photon number operator up to the first side-bands will behave as

$$\begin{aligned} \hat{n}(t) = & \hat{a}_0^\dagger \hat{a}_0 + \hat{a}_b^\dagger \hat{a}_b + \hat{a}_r^\dagger \hat{a}_r + \hat{a}_b^\dagger \hat{a}_0 e^{-i(\Omega + \frac{1}{2}\delta)t} + \hat{a}_0^\dagger \hat{a}_b e^{i(-\Omega + \frac{1}{2}\delta)t} \\ & + \hat{a}_r^\dagger \hat{a}_0 e^{-i(\Omega + \frac{1}{2}\delta)t} + \hat{a}_0^\dagger \hat{a}_r e^{i(\Omega + \frac{1}{2}\delta)t} + \dots, \end{aligned} \tag{2}$$

while the mechanical annihilator will exhibit a closely spaced doublet around the mechanical frequency spaced within  $\delta$  as

$$\hat{b}(t) = \hat{b}_0 + \hat{b}_b e^{-i(\Omega - \frac{1}{2}\delta)t} + \hat{b}_r e^{-i(\Omega + \frac{1}{2}\delta)t} + \dots. \tag{3}$$

Inclusion of 2nd-order side-bands would have generated extra terms in (2) such as  $\hat{a}_{bb}^\dagger \hat{a}_r$  and  $\hat{a}_{rr}^\dagger \hat{a}_b$  and their conjugates as well as  $\hat{a}_{bb}^\dagger \hat{a}_{bb} + \hat{a}_{rr}^\dagger \hat{a}_{rr}$ . For instance,  $\hat{a}_{bb}^\dagger \hat{a}_r$  should have added up to  $\hat{a}_b^\dagger \hat{a}_0$  and so on. These ignored terms all would cause third- or fourth-order corrections to (2), which obviously were dropped.

Here, the average mechanical displacement satisfies

$$b_0 = \langle \hat{b}_0 \rangle = \frac{ig_0 \bar{n}}{i\Omega + \frac{1}{2}\Gamma}. \tag{4}$$

Now, let us get back to the Langevin equation for mechanical motions, which simply is

$$\frac{d}{dt} \hat{b}(t) = \left( -i\Omega - \frac{1}{2}\Gamma \right) \hat{b}(t) - ig_0 \hat{n}(t) + \sqrt{\Gamma} \hat{b}_{\text{in}}(t), \tag{5}$$

where  $\hat{b}_{\text{in}}(t)$  is the operator for mechanical fluctuations. For the purpose of our analysis here, all fluctuations can be discarded since they are irrelevant to the formation of side-band frequencies and average out to zero. Using (2) and (3) we get

$$\begin{aligned} & -i\left(\Omega + \frac{\delta}{2}\right) \hat{b}_r e^{-i(\Omega + \frac{\delta}{2})t} - i\left(\Omega - \frac{\delta}{2}\right) \hat{b}_b e^{-i(\Omega - \frac{\delta}{2})t} \approx -\left(i\Omega + \frac{\Gamma}{2}\right) \hat{b}_r e^{-i(\Omega + \frac{\delta}{2})t} \\ & -\left(i\Omega + \frac{\Gamma}{2}\right) \hat{b}_b e^{-i(\Omega - \frac{\delta}{2})t} - ig_0 \hat{a}_0^\dagger \hat{a}_b e^{-i(\Omega - \frac{\delta}{2})t} - ig_0 \hat{a}_r^\dagger \hat{a}_0 e^{-i(\Omega + \frac{\delta}{2})t} + \dots \end{aligned} \tag{6}$$

From the above, we obtain two key operator equations

$$\begin{aligned} \hat{b}_r &= \frac{-i2g_0}{-i\delta + \Gamma} \hat{a}_r^\dagger \hat{a}_0, \\ \hat{b}_b &= \frac{-i2g_0}{i\delta + \Gamma} \hat{a}_0^\dagger \hat{a}_b. \end{aligned} \tag{7}$$

In a similar manner, the Langevin equation for the photon annihilator is

$$\frac{d}{dt} \hat{a}(t) = \left( i\Delta - \frac{1}{2}\kappa \right) \hat{a}(t) + ig_0 \hat{a}(t) \left[ \hat{b}(t) + \hat{b}^\dagger(t) \right] + \sqrt{\kappa} \hat{a}_{\text{in}}. \tag{8}$$

Using (1) and (3) we obtain

$$\begin{aligned}
 & i\Delta\hat{a}_0e^{i\Delta t} + i\left(\Delta - \Omega + \frac{\delta}{2}\right)\hat{a}_be^{i\left(\Delta - \Omega + \frac{\delta}{2}\right)t} + i\left(\Delta + \Omega + \frac{\delta}{2}\right)\hat{a}_re^{i\left(\Delta + \Omega + \frac{\delta}{2}\right)t} \\
 & \approx \left(i\Delta - \frac{\kappa}{2}\right)\left[\hat{a}_0e^{i\Delta t} + \hat{a}_be^{i\left(\Delta - \Omega + \frac{\delta}{2}\right)t} + \hat{a}_re^{i\left(\Delta + \Omega + \frac{\delta}{2}\right)t}\right] + ig_0\left[\hat{a}_0e^{i\Delta t} + \hat{a}_be^{i\left(\Delta - \Omega + \frac{\delta}{2}\right)t}\right. \\
 & \quad \left. + \hat{a}_re^{i\left(\Delta + \Omega + \frac{\delta}{2}\right)t}\right]\left[\hat{x}_0 + \hat{b}_re^{-i\left(\Omega + \frac{\delta}{2}\right)t} + \hat{b}_be^{-i\left(\Omega - \frac{\delta}{2}\right)t} + \hat{b}_r^\dagger e^{i\left(\Omega + \frac{\delta}{2}\right)t} + \hat{b}_b^\dagger e^{i\left(\Omega - \frac{\delta}{2}\right)t}\right].
 \end{aligned} \tag{9}$$

where  $\hat{x}_0 = \hat{b}_0 + \hat{b}_0^\dagger$ . This will yield the further operator equations as

$$\begin{aligned}
 \frac{\kappa}{2ig_0}\hat{a}_0 &= \hat{a}_0\hat{x}_0 + \hat{a}_b\hat{b}_b^\dagger + \hat{a}_r\hat{b}_r, \\
 \left[\frac{i\left(-\Omega + \frac{\delta}{2}\right) + \frac{\kappa}{2}}{ig_0}\right]\hat{a}_b &= \hat{a}_b\hat{x}_0 + \hat{a}_0\hat{b}_b, \\
 \left[\frac{i\left(\Omega + \frac{\delta}{2}\right) + \frac{\kappa}{2}}{ig_0}\right]\hat{a}_r &= \hat{a}_r\hat{x}_0 + \hat{a}_0\hat{b}_r^\dagger.
 \end{aligned} \tag{10}$$

Now, substituting whatever we have in hand in the second equation of (10), and taking expectation values at the end, we obtain a key algebraic equation in terms of  $\delta$  as

$$i\left(-\Omega + \frac{1}{2}\delta\right) + \frac{1}{2}\kappa = ig_0x_0 - ig_0\sqrt{\bar{n}}\frac{2ig_0\sqrt{\bar{n}}}{i\delta + \Gamma}. \tag{11}$$

with  $x_0 = b_0 + b_0^*$ . Rearrangement of the above gives rise to the equation

$$\delta^2 - [2\Omega + i\gamma + 2g_0x_0]\delta + [(2i\Omega - \kappa)\Gamma + 4g_0^2\bar{n} + 2i\Gamma g_0x_0] = 0, \tag{12}$$

in which  $x_0 = b_0 + b_0^*$  and  $\gamma = \kappa + \Gamma$  is the total optomechanical decay rate<sup>15,17</sup>.

This approximate nature of this equation will yield complex values for  $\delta$  the imaginary value of which has to be discarded. In practice, we observe that imaginary values are much smaller than real values for practical choices of optomechanical parameters. Furthermore, it leaves room to ignore the square terms  $\delta^2$ , to admit the solution

$$\delta = \Re\left[\frac{(2i\Omega - \kappa)\Gamma + 4g_0^2\bar{n} + 2i\Gamma g_0x_0}{2\Omega + i\gamma + 2g_0x_0}\right]. \tag{13}$$

This solution can be put into the more convenient form using (4) and further simplification as

$$\delta(\bar{n}) = \Re\left[\frac{A + B\bar{n}}{C - iD\bar{n}}\right] = \frac{\Re[AC^*] + (B\Re[C] - \Im[A]D)\bar{n}}{|C|^2 - 2\Im[C]D\bar{n} + D^2\bar{n}^2} = \frac{[2\Gamma^2\Omega] + 2\Omega(B - \Gamma D)\bar{n}}{|C|^2 - 4\Omega D\bar{n} + D^2\bar{n}^2}, \tag{14}$$

where

$$\begin{aligned}
 A &= \Gamma(2i\Omega - \kappa) + \frac{4g_0^2\bar{n}(i + 1)\Gamma\Omega}{\Omega^2 + \frac{1}{4}\Gamma^2}, \\
 B &= \frac{4g_0^2\left(\Omega - \frac{1}{2}\Gamma\right)^2}{\Omega^2 + \frac{1}{4}\Gamma^2} = B^*, \\
 C &= i\gamma + 2\Omega, \\
 D &= \frac{4g_0^2\Omega}{\Omega^2 + \frac{1}{4}\Gamma^2} = D^*.
 \end{aligned} \tag{15}$$

In a first approximation,  $A \approx \Gamma(2i\Omega - \kappa)$  can be used. Further simplifications are shown and discussed in the following.

**Limiting cases.** The expression (14) obtained for the SI has interesting properties at the limits of zero and infinite intracavity photon number. We may obtain here after some simplification easily the asymptotic expressions

$$\begin{aligned}\lim_{\bar{n} \rightarrow \infty} \delta(\bar{n}) &\sim \frac{\Omega}{\beta \bar{n}}, \\ \lim_{\bar{n} \rightarrow 0} \delta(\bar{n}) &\sim \frac{2\Gamma^2 \Omega}{4\Omega^2 + \gamma^2} \approx 0,\end{aligned}\quad (16)$$

where  $\beta = 2g_0^2/\Omega^2$ , while noting that  $\Gamma \ll \Omega$  and also for a side-band resolved cavity  $\kappa \ll \Omega$ , together which we have  $\kappa < \gamma \ll \Omega$ .

One should take into account the fact that for Doppler cavities, side-bands normally resolve well enough for a decisive measurement<sup>20</sup>, and the concept of SI is only practically meaningful for side-band resolved cavities. Therefore, the following approximations are valid

$$\begin{aligned}A &\approx 2i\Gamma\Omega, \\ B &\approx 4g_0^2, \\ C &\approx 2\Omega, \\ D &\approx \frac{4g_0^2}{\Omega}, \\ \delta(\bar{n}) &\approx \frac{2\Gamma^2\Omega + 8g_0^2\Omega\bar{n}}{\gamma^2 + 4\Omega^2[1 - 2(g_0/\Omega)^2\bar{n}]^2}.\end{aligned}\quad (17)$$

As long as satisfies  $\bar{n} \ll 2|\Im[C]|/D = \Omega^2/g_0^2$ , then second order term  $\bar{n}^2$  in the denominator of (15) is negligible and can be ignored. Under this regime, the SI varies almost linearly with  $\bar{n}$  as

$$\begin{aligned}\delta(\bar{n}) &\approx \frac{2\Gamma^2\Omega}{4\Omega^2 + \gamma^2} + \frac{8g_0^2\Omega(4\Omega^2 + \gamma^2 + \Gamma^2)}{(\gamma^2 + 4\Omega^2)^2}\bar{n} \\ &\approx \frac{2g_0^2}{\Omega}\bar{n}.\end{aligned}\quad (18)$$

This result is also well in complete agreement with the expression obtained earlier for the SI<sup>15</sup> in the limit of  $g_0 \ll \Omega$  given as  $g_0^2/\Omega$ , considering that a factor of  $\frac{1}{2}$  must be added as a result of different definition of  $\delta$ .

The first immediate conclusion which can be obtained from (18) is that the SI  $\delta$  is always positive, meaning that the detuning frequency of red-sideband should be always a bit larger in magnitude than the blue-sideband. This also agrees with the previous findings of higher-order operator algebra<sup>15</sup>.

Based on (18), in the weakly-coupling limit of  $g_0\sqrt{\bar{n}} < \Gamma$ , the normalized SI defined as  $\bar{\delta} = \delta/\Omega$  can be simply approximated as a function of mechanical frequency as  $\bar{\delta}(\Omega) \approx \frac{1}{2}\Gamma^2/(\Omega^2 + \frac{1}{4}\gamma^2) \approx \frac{1}{2}\Gamma^2/\Omega^2$ . This approximation is fairly convenient in explanation of SI in Raman scattering of various materials which exhibit multiple Raman lines, as shown comprehensively in the Supplementary Information.

**Optimum operation.** The unique mathematical form of (14) which is composed of a first- and second-order polynomials in terms of  $\bar{n}$  respectively, offers a clear maximum at a certain optimum intracavity photon number  $\bar{n}_{\max}$ . To do this, let us first define the dimensionless constants  $\alpha = 4g_0^2/\Gamma^2$  and  $\beta$  already defined under (16),  $\vartheta = \gamma/2\Omega$ , and  $\psi = \Gamma^2/2\Omega^2$ . Then, the SI (17) can be rewritten as

$$\delta(\bar{n}) = \Omega\psi \frac{1 + \alpha\bar{n}}{\vartheta^2 + (1 - \beta\bar{n})^2}.\quad (19)$$

This offers the optimum intracavity photon number and thus the maximum attainable SI as

$$\begin{aligned}\bar{n}_{\max} &= \frac{\sqrt{(\alpha + \beta)^2 + \alpha^2\vartheta^2}}{\alpha\beta} - \frac{1}{\alpha} \approx \frac{1}{\beta} = \frac{\Omega^2}{2g_0^2}, \\ \delta_{\max} &= \delta(\bar{n}_{\max}) \approx \frac{4\Omega^3}{\gamma^2}.\end{aligned}\quad (20)$$

We should take note of the fact that the maximum practically measureable SI, which occurs at the optimum intracavity photon number  $\bar{n}_{\max} = \Omega^2/2g_0^2$ , is actually at the onset of bistability, and under practical conditions, heating due to optical losses in dielectric.

In Fig. 2, variation of SI versus intracavity photon number and in terms of different settings for input parameters  $\{\alpha, \beta, \vartheta\}$  is illustrated.

**Operation regimes.** Another very important result which can be drawn from the above discussions, is marking the boundaries of linear, weakly nonlinear, and strongly nonlinear interaction regimes in quantum optomechanics. This follows by normalizing  $\delta$  with respect to the mechanical frequency  $\Omega$  first, as  $\bar{\delta} = \delta/\Omega$ .

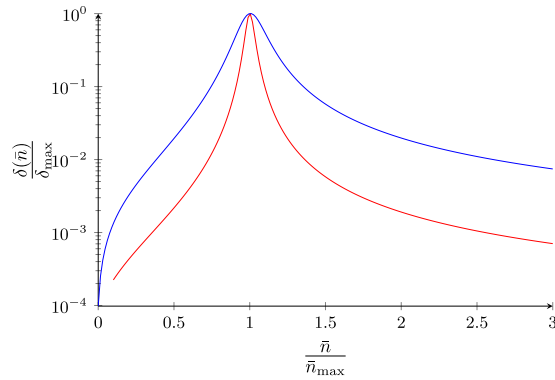


**Figure 2.** Variation of SI around the maximum point in terms of various settings of parameters: (blue)  $\alpha = 0.1$ ,  $\beta = 10^{-3}$ , and  $\vartheta = 0.1$  (red)  $\alpha = 0.1$ ,  $\beta = 10^{-2}$ , and  $\vartheta = 3.16 \times 10^{-2}$ . Normalization on the vertical axis has been done to drop dependence of  $\delta$  on  $\Omega\psi$  in (19). The behavior versus intracavity photon number  $\bar{n}$  is clearly not Lorentzian.

- Fully Linear: This regime is easily given by  $\bar{n} \ll \bar{n}_{\max}$ , where intracavity photon number is essentially too low to cause any appreciable SI. Here, the behavior of normalized SI is proportional to  $\bar{n}$ .
- Weakly Nonlinear: This regime is next given by  $\bar{n} \sim \bar{n}_{\max}$  around the optimum operation point, where the SI rises to attain a maximum. The behavior of normalized SI is nearly Lorentzian centered at  $\bar{n} = \bar{n}_{\max}$ , with an intracavity photon number linewidth of  $\Delta\bar{n} = \vartheta\bar{n}_{\max}$ .
- Strongly Nonlinear: This regime at larger intracavity photon numbers satisfying  $\bar{n} \gg \bar{n}_{\max}$  will push the system into strongly nonlinear regime where the SI quickly start to fade away. Here, the behavior of normalized SI is inversely proportional to  $\bar{n}$ .

These three behaviors in above operation regimes can be respectively displayed as

$$\begin{aligned} \bar{\delta}(\bar{n}) &\sim \left(\frac{\bar{n}}{\bar{n}_{\max}}\right)\bar{\delta}_{\max}, & \bar{n} \ll \bar{n}_{\max}, \\ \bar{\delta}(\bar{n}) &\sim \left\{1 + \vartheta^{-2}\left(\frac{\bar{n}}{\bar{n}_{\max}} - 1\right)^2\right\}^{-1}\bar{\delta}_{\max}, & \bar{n} \sim \bar{n}_{\max}, \\ \bar{\delta}(\bar{n}) &\sim \left(\frac{\bar{n}_{\max}}{\bar{n}}\right)\bar{\delta}_{\max}, & \bar{n} \gg \bar{n}_{\max}. \end{aligned} \tag{21}$$

**Fundamental symmetries.** It is easy to verify that the SI does not violate the two fundamental symmetries of the nature. Here, both the time-reversal symmetry as well as the conservation of energy are preserved. The energy of scattered red- and blue- photons  $\hbar\omega \mp \hbar\Omega$  is normally expected to be within the energy of one phonon  $\hbar\Omega$  where  $\omega$  is the angular frequency of incident electromagnetic radiation. Per every annihilated photon, exactly one phonon is either annihilated, giving rise to a blue-shifted photon, or one phonon is created, giving rise to a red-shifted photon.

However, not all phonons are having exactly the same energies. This is permissible by the non-vanishing mechanical linewidth  $\Gamma > 0$  of the cavity. One should expect that once this quantity vanishes, the SI is gone, since it is by (19) proportional to  $\Gamma^2$ . Hence, basically it should be not contradictory to have a possible non-zero SI.

With regard to the time-reversal symmetry, one must take notice of the fact that all optical frequencies are physically positive, since we first must move back out of the rotating reference frame. For instance, the blue- and red-scattered photons have frequencies given by  $\omega_b = \omega_c + \Omega - \frac{1}{2}\delta$  and  $\omega_r = \omega_c - \Omega - \frac{1}{2}\delta$ . Therefore, blue and red processes are not time-reversed processes of each other, as they both stay on the positive frequency axis. Negative frequency images corresponding to both processes do however exist and exactly satisfy the time-reversal.

**Optomechanical experiments.** To the best knowledge of the author, at least two very high resolution optomechanical experiments on side-band resolved samples, reveal the existence of SI, shown in Table 1. One experiment<sup>22</sup> exhibits a normalized SI of  $(3.5 \pm 0.9) \times 10^{-6}$ , equivalent to  $\delta = 2\pi \times (142 \pm 36)$  Hz with  $\Omega = 2\pi \times 40.5968$  MHz. There exists a much more recent experiment, where the observed normalized SI is much stronger  $(9.23 \pm 0.66) \times 10^{-4}$ <sup>23</sup>.

Inclusion of higher-order side-bands up to the  $n$ -th order would have caused an algebraic equation of the order  $2n$  in place of the quadratic (12), which is in general impossible to solve explicitly. Furthermore, the numerical advantage of treating such a generalized case would be only minor. With regard to the imaginary part  $\Im[\delta]$  which was discarded, even if it were non-zero in the exact analysis, it could have resulted for instance in modification of linewidths. This calls for a deeper study of this subject, and it is also worth mentioning that the asymmetry of linewidths in optomechanics has recently been studied elsewhere in the linearized regime<sup>24</sup>.

Experiment	SI $\delta/(2\pi)$	Normalized SI $\bar{\delta} = \delta/\Omega$	Remarks
Schleisser <i>et al.</i> <sup>22</sup>	$142 \pm 36$ Hz	$(3.5 \pm 0.9) \times 10^{-6}$	Resonant pump <sup>a</sup>
Sudhir <i>et al.</i> <sup>23</sup>	$3.97 \pm 0.284$ kHz	$(9.23 \pm 0.66) \times 10^{-4}$	Out-of-loop heterodyne spectra <sup>b</sup>

**Table 1.** Side-band inequivalence in absolute values and normalized quantities in optomechanical experiments. Both experiments are carried out on side-band resolved cavities and have sufficiently high resolution to look for deviations from ideal expected case. Further examples are analyzed and discussed in Supplementary Information. <sup>a</sup>Analysis done on Fig. 5b<sup>22</sup> and the data corresponding to the side-bands at resonant  $\Delta = 0$  pumping, which are much more visible and reliable. For near-blue resonant pump with  $\Delta \approx -\Omega$  deviations lie within the error margin and are thus inconclusive. Coordinates of side-band Lorentzians were taken from ultra high-resolution digitalization of the graph. <sup>b</sup>Analysis done on the open-loop configuration with no feedback in Fig. 4b<sup>23</sup>.

Material	Normalized SI $\bar{\delta} = \delta/\Omega$	Remarks
MoTe <sub>2</sub>	$(7 \pm 0.8) \times 10^{-2}$	6-layer <sup>35</sup>
MoS <sub>2</sub>	$(3 \pm 1) \times 10^{-3}$	6-layer <sup>36</sup>
	$(7.8 \pm 1.5) \times 10^{-3}$	flake <sup>37</sup>
CNT <sup>a</sup>	$(6.0 \pm 2.1) \times 10^{-3}$	(10, 5) SC <sup>b27</sup>
	$(2 \pm 1) \times 10^{-3}$	1st-order; SC <sup>b28</sup>
	$(1.22 \pm 0.13) \times 10^{-2}$	2nd-order; SC <sup>b28</sup>
	$(1.5 \pm 0.18) \times 10^{-2}$	single-wall <sup>29</sup>
	$(2.11 \pm 0.35) \times 10^{-2}$	single-wall <sup>30</sup>
Gr <sup>c</sup>	$(8.0 \pm 1.6) \times 10^{-3}$	4-layer <sup>39</sup>
	$(5 \pm 1.7) \times 10^{-3}$	3-layer <sup>39</sup>
	$(1.63 \pm 0.48) \times 10^{-2}$	(1, 2)-twisted <sup>40</sup>
	$(2.2 \pm 1.09) \times 10^{-2}$	C <sub>31</sub> (1, 3)-twisted <sup>d40</sup>
	$(3.6 \pm 1.8) \times 10^{-2}$	C <sub>32</sub> (1, 3)-twisted <sup>d40</sup>
C	$(1.15 \pm 0.57) \times 10^{-2}$	Bulk <sup>41</sup>
S <sup>e</sup>	$(1.03 \pm 0.25) \times 10^{-2}$	1st-order; grains <sup>37</sup>
	$(7.2 \pm 1.8) \times 10^{-3}$	2nd-order; grains <sup>37</sup>
Ethanol	$(1.8 \pm 0.4) \times 10^{-3}$	1st-order; EX <sup>f42</sup>
H <sub>2</sub>	$(4.7 \pm 0.223) \times 10^{-4}$	MOM <sup>g43</sup>
Gr	$(2.67 \pm 0.074) \times 10^{-3}$	Pop = 7.0 mW <sup>b44</sup>
	$(1.67 \pm 0.165) \times 10^{-3}$	Pop = 3.8 mW <sup>b44</sup>
	$(0.67 \pm 0.603) \times 10^{-3}$	Pop = 1.8 mW <sup>b44</sup>
B4 <sup>i</sup>	$(3.4 \pm 0.18) \times 10^{-3}$	1090 nm line <sup>45,46</sup>
SRA <sup>k</sup>	$(1.424 \pm 0.01) \times 10^{-3}$	Yb-doped fiber <sup>47,48</sup>

**Table 2.** Side-band inequivalence in Raman spectra of various materials, computed based on the highest-resolution available measurements. The last four rows under the single separating horizontal line are obtained by direct calculation on available high-resolution measurement data. Confidence interval for these last three measurements is remarkably significant, leaving no doubt in existence of SI. Further examples are analyzed and discussed in Supplementary Information. <sup>a</sup>CNT: Carbon Nano-tube. <sup>b</sup>SC: Semiconducting. <sup>c</sup>Gr: Graphene. <sup>d</sup>1.96 eV excitation. <sup>e</sup>S: Sulphur. <sup>f</sup>EX: Excitation at 532 nm. <sup>g</sup>MOM: Molecular Optical Modulation; Measurement at 1015 kPa done on ortho-H<sub>2</sub>, which has a 17.6 THz rotational motion frequency. Experimental data received from the authors through private communication. <sup>h</sup>3ps Ultrafast Excitation; Experimental data received from the authors through private communication. Data has to be shifted to adjust for  $\delta(0) = 0$ , and exhibits a linear rate of  $3.867 \times 10^{-4}/\text{mW}$  versus input power, in agreement with the weakly nonlinear regime of (21) as  $\delta(\bar{n}) \propto \bar{n}$ . <sup>i</sup>B4: Single Biphenyl-4-thiol molecule in monolayer confined to optical picocavity; Experimental data available online<sup>46</sup>. <sup>j</sup>4-point moving average applied. Gaussian 10-point filtering results in the much larger value of  $1.06 \times 10^{-2}$ . <sup>k</sup>SRA: Stimulated Raman Amplifier; Experimental data available online<sup>48</sup>.

**Raman scattering.** Remarkably, the Stokes and anti-Stokes peaks of Raman spectra also exhibit the same phenomenon of SI. This has so far skipped the attention since normally the nonlinear interaction rate causing the formation of Raman scattering is too small for majority of bulk materials and liquids. Again, a full linear theory of Raman scattering<sup>25</sup> disallows SI. However, with the recent advent of low-dimensional materials, optical nonlinear interactions leading to Raman scattering<sup>26,31–33,38</sup> and Kerr effect<sup>34</sup> are available at much stronger rates.

Table 2 provides a summary of measurable SI based on the reported Raman scattering of different materials. Calculations of normalized SI and errors are done according to the best possible resolution of measurement graphs. It has to be noted that for every given material, the SI is a strong function of scattering order, excitation

wavelength, polarization, angle of incidence, as well as intensity. Therefore, it is not possible to reconstruct a fit to varying function for  $\delta$  as (19). However, the existence of a previously unnoticed SI, which is always leaning toward the red side-band seems to be conclusive. Therefore, a rigorous quantum theory of SI for Raman scattering from continuum optomechanics is yet to be developed, such as the one recently developed for materials<sup>25</sup>.

In the end and following the above, let us now plug-in (4) and (7) into the first of (10). Some simplifications, while ignoring the inequilibrium quantum thermal effects on the population of side-bands, gives the equation

$$\bar{n}_r - \bar{n}_b \approx \left( \frac{\Omega \bar{n}}{\Omega^2 + \frac{1}{4}\Gamma^2} \right) \delta \approx \frac{\bar{n}}{\Omega} \delta. \quad (22)$$

Here,  $\bar{n}_r = |\bar{a}_r|^2$  and  $\bar{n}_b = |\bar{a}_b|^2$  respectively refer to the number of scattered photons unto red and blue side-bands. Then, from (19), and assuming that  $\bar{N} = (\bar{n}_r - \bar{n}_b)/\bar{n}$  denotes the normalized asymmetry of side-bands, we get

$$\bar{N}(\bar{n}) = \frac{\psi(1 + \alpha\bar{n})}{\vartheta^2 + (1 - \beta\bar{n})^2}. \quad (23)$$

Accordingly the asymmetry is increases up to a positive maximum, before decreasing back to zero at sufficiently high powers.

**Side-band inequivalence in other areas.** Finally, it is easy to see that the same nonlinear symmetry breaking can lead to asymmetry in the particle pair production or parametric down conversion, which can be considered as the dual of optomechanical process<sup>49,50</sup>. In order to observe this fact, consider an optomechanical system with a mechanical frequency roughly double the optical frequency  $\Omega \approx 2\omega$ . If the mechanics is driven strong enough at the frequency  $\Omega$ , then the effective interaction Hamiltonian will be simply  $\mathbb{H}_{\text{eff}} = i\hbar g(\hat{a}^\dagger \hat{a}^\dagger \hat{b} - \hat{a} \hat{a} \hat{b}^\dagger)$ , where a phonon with energy  $\hbar\Omega$  dissociates into two photons with energies  $\hbar(\omega \pm \delta)$  with  $\delta$  representing the corresponding symmetry breaking in pair frequencies caused by SI. Parametric down conversion for phonons has recently been observed and reported, too<sup>51</sup>.

Also, based on the duality of effective interaction Hamiltonian in linear electro-optic modulation (within the validity of rotating wave approximation), with the optomechanical Hamiltonian<sup>52-54</sup>, one could predict that the same nonlinear inequivalence to appear in relevant experiments, too. As an example, optical modulation of Hydrogen<sup>43</sup> is already shown in Table 2 to exhibit this phenomenon. Hence, further implications could be expected in communications technology and filtering, where precise positioning of side-bands are of importance. Similar arguments should be valid for enhanced Raman scattering of single molecules by localized plasmonic resonances as well<sup>55</sup>.

## Conclusions

We presented a complete analysis of SI in quantum optomechanics, and showed it undergoes a maximum and obtained closed-form expressions for optimum intracavity photon number as well as maximum attainable SI. We classified the operation into the linear, weakly nonlinear, and strongly nonlinear regimes, in which the behavior of system is markedly different. The results of this investigation can provide the accuracy constraints as well as necessary experimental set up to resolve the elusive SI. Analysis of high resolution measurements of Raman scattering for different materials confirms the existence of SI. One could speculate that precise measurement of the variation of side-band inequivalence in terms of various system parameters could provide further insight into unexplored nonlinear properties of different material.

## References

1. Aspelmeyer, M., Kippenberg, T. J. & Marquardt, F. Cavity optomechanics. *Rev. Mod. Phys.* **86**, 1391 (2014).
2. Kippenberg, T. J. & Vahala, K. J. Cavity optomechanics: Back-action at the mesoscale. *Science* **321**, 1172 (2008).
3. Aspelmeyer, M., Kippenberg, T. & Marquardt, F. *Cavity Optomechanics: Nano- and Micromechanical Resonators Interacting with Light* (Springer, Berlin, 2014).
4. Meystre, P. A short walk through quantum optomechanics. *Ann. Phys.* **525**, 215 (2013).
5. Bowen, W. P. & Milburn, G. J. *Quantum Optomechanics* (CRC Press, Boca Raton, 2016).
6. Gu, W. J., Yi, Z., Sun, L.-H. & Yan, Y. Enhanced quadratic nonlinearity with parametric amplifications. *J. Opt. Soc. Am. B* **35**, 652 (2018).
7. Zhang, J. S. & Chen, A.-X. Enhancing quadratic optomechanical coupling via nonlinear medium and lasers. *Phys. Rev. A* **99**, 013843 (2019).
8. Hossein-Zadeh, M. & Vahala, K. J. Observation of optical spring effect in a microtoroidal optomechanical resonator. *Opt. Lett.* **32**, 1611 (2007).
9. Huang, K. & Hossein-Zadeh, M. Direct stabilization of optomechanical oscillators. *Opt. Lett.* **42**, 1946 (2017).
10. Akram, M. J., Aranas, E. B., Bullier, N. P., Lang, J. E. & Monteiro, T. S. Two-timescale stochastic Langevin propagation for classical and quantum optomechanics. *Phys. Rev. A* **98**, 063827 (2018).
11. Purdy, T. P. *et al.* Optomechanical Raman-ratio thermometry. *Phys. Rev. A* **92**, 031802(R) (2015).
12. Purdy, T. P., Grutter, K. E., Srinivasan, K. & Taylor, J. M. Quantum correlations from a room-temperature optomechanical cavity. *Science* **356**, 1265 (2017).
13. Marquardt, F., Chen, J. P., Clerk, A. A. & Girvin, S. M. Quantum theory of cavity-assisted sideband cooling of mechanical motion. *Phys. Rev. Lett.* **99**, 093902 (2007).
14. Wilson-Rae, I., Nooshi, N., Zwerger, W. & Kippenberg, T. J. Theory of ground state cooling of a mechanical oscillator using dynamical backaction. *Phys. Rev. Lett.* **99**, 093901 (2007).
15. Khorasani, S. Method of higher-order operators for quantum optomechanics. *Sci. Rep.* **8**, 11566 (2018).
16. Khorasani, S. Higher-order interactions in quantum optomechanics: Revisiting theoretical foundations. *Appl. Sci.* **7**, 656 (2017).
17. Khorasani, S. Higher-order interactions in quantum optomechanics: Analytical solution of nonlinearity. *Photonics* **4**, 48 (2017).
18. Khorasani, S. Higher-order interactions in quantum optomechanics: Analysis of quadratic terms. *Sci. Rep.* **8**, 16676 (2018).
19. Khorasani, S. Solution of cross-Kerr interaction combined with parametric amplification. *Sci. Rep.*, accepted (2019).



20. Khorasani, S. Momentum-field interactions beyond standard quadratic optomechanics. In *Quantum Mechanics: Theory, Analysis, and Applications* (ed. Arbab, A. I.) 1–17 (Nova Science Publishers, 2018).
21. Khorasani, S. & Cabon, B. Theory of Optimal Mixing in Directly Modulated Laser Diodes. *Scientia Iranica* **16**, 157 (2009).
22. Schliesser, A., Rivière, R., Anetsberger, G., Arcizet, O. & Kippenberg, T. J. Resolved-sideband cooling of a micromechanical oscillator. *Nat. Phys.* **4**, 415 (2008).
23. Sudhir, V. *et al.* Appearance and Disappearance of Quantum Correlations in Measurement-Based Feedback Control of a Mechanical Oscillator. *Phys. Rev. X* **7**, 011001 (2017).
24. Otterstrom, N. T., Behunin, R. O., Kittlaus, E. A. & Rakich, P. T. Optomechanical cooling in a continuous system. *Phys. Rev. X* **8**, 041034 (2018).
25. Rakich, P. & Marquardt, F. Quantum theory of continuum optomechanics. *New J. Phys.* **20**, 045005 (2018).
26. Dresselhaus, M. S., Dresselhaus, G. & Eklund, P. Raman scattering in fullerenes. *J. Raman Spect.* **27**, 351 (1996).
27. Souza Filho, A. G. *et al.* Stokes and anti-Stokes Raman spectra of small-diameter isolated carbon nanotubes. *Phys. Rev. B* **69**, 115428 (2004).
28. Dresselhaus, M. S., Dresselhaus, G., Saito, R. & Jorio, A. Raman spectroscopy of carbon nanotubes. *Phys. Rep.* **409**, 47 (2005).
29. Jorio, A. *et al.* Joint density of electronic states for one isolated single-wall carbon nanotube studied by resonant Raman scattering. *Phys. Rev. B* **63**, 245416 (2001).
30. Chen, Y. *et al.* Helicity-dependent single-walled carbon nanotube alignment on graphite for helical angle and handedness recognition. *Nat. Commun.* **4**, 2205 (2013).
31. Tan, P.-H. ed. *Raman Spectroscopy of Two-dimensional Materials* (Springer, Singapore, 2019).
32. Shao, F. & Zenobi, R. Tip-enhanced Raman spectroscopy: principles, practice, and applications to nanospectroscopic imaging of 2D materials. *Anal. Bioanal. Chem.* **411**, 37 (2019).
33. Jorio, A., Saito, R., Dresselhaus, G. & Dresselhaus, M. S. *Raman Spectroscopy in Graphene Related Systems*. (Wiley-VCH, Weinheim, 2011).
34. Khorasani, S. Third-order optical nonlinearity in two-dimensional transition metal dichalcogenides. *Commun. Theor. Phys.* **70**, 334 (2018).
35. Goldstein, T. *et al.* Raman scattering and anomalous Stokes–anti-Stokes ratio in MoTe<sub>2</sub> atomic layers. *Sci. Rep.* **6**, 28024 (2016).
36. Zhang, X. *et al.* Phonon and Raman scattering of two-dimensional transition metal dichalcogenides from monolayer, multilayer to bulk material. *Chem. Soc. Rev.* **44**, 2757 (2015).
37. Tuschel, D. Raman spectroscopy and imaging of low energy phonons. *Spectroscopy* **30**, 18 (2015).
38. Saito, R., Hofmann, M., Dresselhaus, G., Jorio, A. & Dresselhaus, M. S. Raman spectroscopy of graphene and carbon nanotubes. *Adv. Phys.* **60**, 413 (2011).
39. Wu, J.-B., Lin, M.-L., Cong, X., Liua, H.-N. & Tan, P.-H. Raman spectroscopy of graphene-based materials and its applications in related devices. *Chem. Soc. Rev.* **47**, 1822 (2018).
40. Wu, J.-B. *et al.* Resonant Raman spectroscopy of twisted multilayer graphene. *Nat. Commun.* **5**, 5309 (2014).
41. Tan, P.-H. *et al.* The shear mode of multilayer graphene. *Nat. Mater.* **11**, 294 (2012).
42. <https://www.nanophoton.net/raman/raman-spectroscopy.html>.
43. Zaitsev, S.-I., Izaki, H., Tsuchiya, T. & Imasaka, T. Continuous-wave phase-matched molecular optical modulator. *Sci. Rep.* **6**, 20908 (2016).
44. Ferrante, C. *et al.* Raman spectroscopy of graphene under ultrafast laser excitation. *Nat. Commun.* **9**, 308 (2018).
45. Benz, F. *et al.* Single-molecule optomechanics in “picocavities”. *Science* **354**, 726 (2016).
46. Benz, F. *et al.* Single-molecule optomechanics in “picocavities”. [Data set] *Apollo*, <https://doi.org/10.17863/CAM.1675> (2016).
47. Runcorn, T. H., Murray, R. T. & Taylor, J. R. Highly efficient nanosecond 560 nm source by SHG of a combined Yb-Raman fiber amplifier. *Opt. Express* **26**, 4440 (2018).
48. Runcorn, T. H., Murray, R. T. & Taylor, J. R. Highly efficient nanosecond 560 nm source by SHG of a combined Yb-Raman fiber amplifier. [Data set] *Zenodo* <https://doi.org/10.5281/zenodo.1166082> (2018).
49. Di Stefano, O. *et al.* Interaction of mechanical oscillators mediated by the exchange of virtual photon pairs. *Phys. Rev. Lett.* **122**, 030402 (2019).
50. Jansen, E., Machado, J. D. P. & Blanter, Y. M. Realization of a degenerate parametric oscillator in electromechanical systems. *Phys. Rev. B* **99**, 045401 (2019).
51. Nabhholz, U., Schatz, F., Mehner, J. E. & Degenfeld-Schonburg, P. Spontaneous parametric down-conversion induced by non-degenerate phononic three-wave mixing in a scanning MEMS micro mirror. *Sci. Rep.* **9**, 3997 (2019).
52. Capmany, J. & Fernández-Pousa, C. R. Quantum model for electro-optical phase modulation. *J. Opt. Soc. Am. B* **27**, A119 (2010).
53. Schmidt, M. K., Esteban, R., González-Tudela, A., Giedke, G. & Aizpurua, J. Quantum mechanical description of Raman scattering from molecules in plasmonic cavities. *ACS Nano* **10**, 6291 (2016).
54. Lombardi, A. *et al.* Pulsed molecular optomechanics in plasmonic nanocavities: From nonlinear vibrational instabilities to bond-breaking. *Phys. Rev. X* **8**, 011016 (2018).
55. Roelli, P., Galland, C., Piro, N. & Kippenberg, T. J. Molecular cavity optomechanics as a theory of plasmon-enhanced Raman scattering. *Nature Nanotech.* **11**, 164 (2016).

## Acknowledgements

This article is dedicated to the celebrated artist, Anastasia Huppmann.

## Additional Information

**Supplementary information** accompanies this paper at <https://doi.org/10.1038/s41598-019-45580-7>.

**Competing Interests:** The author declares no competing interests.

**Publisher’s note:** Springer Nature remains neutral with regard to jurisdictional claims in published maps and institutional affiliations.



**Open Access** This article is licensed under a Creative Commons Attribution 4.0 International License, which permits use, sharing, adaptation, distribution and reproduction in any medium or format, as long as you give appropriate credit to the original author(s) and the source, provide a link to the Creative Commons license, and indicate if changes were made. The images or other third party material in this article are included in the article’s Creative Commons license, unless indicated otherwise in a credit line to the material. If material is not included in the article’s Creative Commons license and your intended use is not permitted by statutory regulation or exceeds the permitted use, you will need to obtain permission directly from the copyright holder. To view a copy of this license, visit <http://creativecommons.org/licenses/by/4.0/>.

© The Author(s) 2019